many of the problems traditionally associated with the numerical solution of singular integral equations. The ANM boundary element formulation leads to accurate solutions and rapid numerical convergence and is free from the ambiguity present in many traditional singularity methods.

The input gust field in this problem is composed of an infinite row of vortices with viscous central cores. Each component vortex in the row is based on a new analytical model, which calculates trailing vortex structure based on prescribed blade loading distribution and strength. In this model problem, vortex properties are calculated for an assumed elliptic lift distribution with net lift coefficient of unity. There are no free parameters, such as core size, in this vortex model. All vortex properties are determined uniquely as a result of the assumed generating lift distribution. Thus, the present vortex model is applicable to both independently generated and self-generated vortices in the study of BVI.

Calculations for the radiated acoustic pressure are given, which exhibit the behavior expected from a two-dimensional BVI, and the effect of varying the vortex miss distance on the peak radiated acoustic pressure is investigated.

Acknowledgments

The first author was supported by a Graduate Student Researchers Program Fellowship from the NASA Langley Research Center with Thomas F. Brooks serving as Technical Monitor. The second author is supported by a Graduate Student Researchers Program Fellowship from the NASA Ames Research Center with William G. Warmbrodt serving as Technical Monitor. The authors would like to thank Todd R. Quackenbush at Continuum Dynamics, Inc., for helpful discussions while the manuscript was in preparation.

References

[1]Caradonna, F. X., Laub, G. H., and Tung, C., "An Experimental Investigation of the Parallel Blade-Vortex Interaction," *Proceedings of the 10th European Rotorcraft Forum* (The Hague, The Netherlands), American Helicopter Society, Alexandria, VA, 1984.

[2]Prichard, D., Burley, C., and Boyd, D. D., Jr., "Computational Techniques for Improved Blade Vortex Interaction Modeling," *Proceedings of the 51st Annual Forum of the American Helicopter Society* (Fort Worth, TX), American Helicopter Society, Alexandria, VA, 1995.

[3]Kitaplioglu, C., and Caradonna, F. X., "Aerodynamics and Acoustics of Blade-Vortex Interaction Using an Independently Generated Vortex," *Proceedings of the American Helicopter Society Aeromechanics Specialists Conference* (San Francisco, CA), American Helicopter Society, Alexandria, VA, 1994.

[4]Farassat, F., and Brentner, K. S., "The Uses and Abuses of the Acoustic Analogy in Helicopter Rotor Noise Prediction," *Journal of the American Helicopter Society*, Vol. 33, Jan. 1988, pp. 29–36.

[5]Brentner, K., "Prediction of Helicopter Rotor Discrete Frequency Noise," NASA TR TM-87721, Oct. 1986.

[6]Ffowcs Williams, J. E., "The Acoustic Analogy—Thirty Years On," *Journal of Applied Mathematics*, Vol. 32, 1984.

[7]Kirchhoff, G. R., "Towards a Theory of Light Rays," *Annals of Physical Chemisty*, Vol. 18, 1883, pp. 663–695.

[8]Pierce, A. D., *Acoustics: An Introduction to Its Physical Principals and Applications*, Acoustical Society of America, New York, 1989, Chap. 5.

[9]Farassat, F., and Myers, M., "Extension of Kirchhoff's Formula to Radiation from Moving Surfaces," *Journal of Sound and Vibration*, Vol. 123, 1988, pp. 451–460.

[10]Betz, A., "Behavior of Vortex Systems," NACA TR TM-713, June 1933.

[11]Mason, W. H., and Marchman, J. F., III, "Far-Field Structure of Aircraft Wake Turbulence," *Journal of Aircraft*, Vol. 12, No. 2, 1973, pp. 86–92.

[12]Hoffmann, E., and Joubert, P. N., "Turbulent Line Vortices," *Journal of Fluid Mechanics*, Vol. 16, 1963, pp. 395–411.

[13]Rule, J., and Bliss, D., "Prediction of Turbulent Trailing Vortex Structure for Rotorcraft Blade-Vortex Interaction," *Proceedings of the 51st Annual Forum of the American Helicopter Society* (Fort Worth, TX), American Helicopter Society, Alexandria, VA, 1995.

[14]Milne-Thomson, L. M., *Theoretical Hydrodynamics*, Macmillan, New York, 1968, Chap. 13.

[15]Garrick, I. E., *Nonsteady Wing Characteristics, Aerodynamics of Aircraft Components at High Speed*, Vol. 7, Princeton Univ. Press, Princeton, NJ, 1957, Sec. F.

[16]Ashley, H., and Landahl, M., *Aerodynamics of Wings and Bodies*, Dover, Mineola, NY, 1965, Chap. 1.

[17]Morse, P. M., and Feshbach, H., *Methods of Theoretical Physics*, McGraw–Hill, New York, 1953.

[18]Kellogg, O. D., *Foundations of Potential Theory*, Dover, Mineola, NY, 1953, Chap. 2.

[19]Garrick, I. E., "On Moving Sources in Nonsteady Aerodynamics and in Kirchhoff's Formula," *Proceedings of the First U.S. National Congress of Applied Mechanics* (Chicago, IL), American Society of Mechanical Engineers, 1951.

[20]Morino, L., "A General Theory of Unsteady Compressible Potential Aerodynamics," NASA TR CR 2464, Langley Research Center, Dec. 1974.

[21]Larmor, J., "On the Mathematical Expression of the Principle of Huygens," *Proceedings of the London Mathematical Society*, Vol. 2, No. 1, 1903, pp. 1–13.

[22]Bliss, D. B., and Epstein, R. J., "A Novel Approach to Aerodynamic Analysis Using Analytical/Numerical Matching," *Proceedings of the 13th AIAA Applied Aerodynamics Conference* (San Diego, CA), AIAA, Washington, DC, 1995.

[23]Epstein, R. J., and Bliss, D. B., "An Acoustic Boundary Element Method Using Analytical/Numerical Matching," *Journal of the Acoustical Society of America*, Vol. 101, No. 1, 1997, pp. 92–106.

[24]Bliss, D. B., and Epstein, R. J., "Novel Approach to Aerodynamic Analysis Using Analytical/Numerical Matching," *AIAA Journal*, Vol. 34, No. 11, 1996, pp. 2225–2232.

[25]Epstein, R. J., and Bliss, D. B., "An Aeroacoustic Boundary Element Method Using Analytical/Numerical Matching," *Proceedings of the 1st Joint CEAS/AIAA Aeroacoustics Conference* (Munich, Germany), 1995.

[26]Epstein, R. J., and Bliss, D. B., "Aeroacoustic Boundary Element Method Using Analytical/Numerical Matching," *AIAA Journal*, Vol. 35, No. 2, 1997, pp. 244–254.

S. Fleeter
Associate Editor

Box-Length Requirements for Simulation of Sound from Large Structures in Jets

E. J. Avital* and N. D. Sandham†
Queen Mary and Westfield College, London E1 4NS, England, United Kingdom

Introduction

LARGE-SCALE structures in the mixing region of jets are known to be dominant sound producers in forced jets.[1,2] These structures can be modeled as instability waves, initially growing, then saturating and decaying. Thus one can refer to them as wave packets. This kind of model was used to determine the magnitude of the radiated sound.[3] It was also used to explain the appearance of superdirectivity in the sound field of low subsonic jets,[4] as had been found experimentally.[2] When it comes to simulating the sound generated by a large-scale structure, one problem is that one is confined to the use of a finite-size computational box (see Fig. 1). In this study it is assumed that the large-scale structure of the shear layer has been successfully simulated inside the finite box. Then the question is whether the box is long enough in the longitudinal direction to include a sufficient portion of the acoustic source to get an accurate description of the sound field. The answer depends partly on the quality of the boundary conditions applied on the box sides. However, we assume that the boundary conditions are so accurate that no distortion is created in the sound field due to them. Thus this study gives the minimum required computational length scale that is determined only by the physical mechanism of the sound generation.

Only two attempts to use a wave-packet model to determine the required computational box are reported in the literature. The first,

Received Oct. 26, 1996; revision received Jan. 15, 1997; accepted for publication Jan. 17, 1997.

*Ph.D. Student, Department of Engineering, Mile End Road. Student Member AIAA.

†Lecturer, Department of Engineering, Mile End Road. Member AIAA.

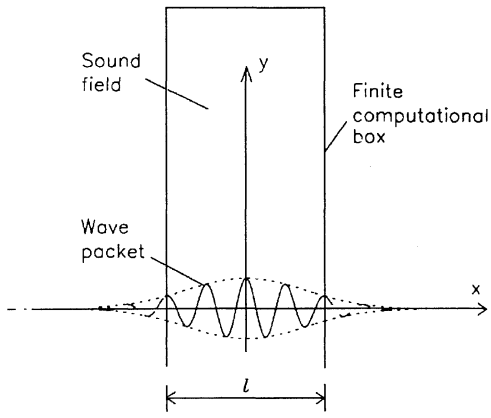

Fig. 1 Schematic description of the problem.

by Crighton,[5] used the work of Crighton and Huerre[4] to give a rough estimate for a low-subsonic Gaussian wave packet. The second, by Mitchell et al.,[6] used an acoustic analogy with a Gaussian wave-packet source to determine the effect of the computational box length on their sound calculations for an axisymmetric supersonic jet. This Note fills the gap left by these studies and gives a general solution to the problem by investigating the effect of the connvective Mach number and different possible shapes of the wave packet on the required computational box length. Because the boundary conditions are assumed to be so accurate that no distortion in the sound directivity and magnitude is created, the only reasonable parameter by which one can check the effect of the finite length of the computational box is the total acoustic power output emitted by the source. This study gives simple analytical expressions for the acoustic power output and the required box length for the low-subsonic and supersonic cases.

Large-Scale Model, Infinite Box

The analysis will follow the model suggested by Crighton and Huerre.[4] The acoustic source is represented by a wave packet on the lower side of the box, as in Fig. 1. The space and time arguments are normalized, and so, the pressure fluctuations of the sound field are taken as $p(x, y)\exp(-it)$. A two-dimensional wave equation of a stationary medium is assumed to be the governing equation; then, one can derive the following equation and boundary condition:

$$\frac{\partial^2 p}{\partial x^2} + \frac{\partial^2 p}{\partial y^2} + M_c^2 p = 0, \qquad -\infty < x < \infty, y \geq 0 \tag{1}$$

$$p(x, y = 0) = A(\varepsilon x)e^{ix} \tag{2}$$

where $M_c \equiv \omega_m/(k_m c_0)$ is the convective Mach number; ω_m and k_m are the wave packet's dimensional main frequency and number, respectively; A is the envelope shape function, and it is taken that $\varepsilon < \mathcal{O}(1)$. Crighton and Huerre[4] showed that a solution of Eqs. (1) and (2) that obeys the radiation boundary condition at infinity can be expressed as

$$p(x, y) = \frac{1}{\varepsilon}\int_{-\infty}^{\infty} \hat{A}\left(\frac{k-1}{\varepsilon}\right)e^{ikx-\gamma y}\,\mathrm{d}k \tag{3}$$

$$\gamma = \begin{cases} \sqrt{k^2 - M_c^2}, & |k| \geq M_c \\ -i\sqrt{M_c^2 - k^2}, & |k| \leq M_c \end{cases} \tag{4}$$

where $\hat{A}$ is the Fourier transform of A. Two kinds of wave packets are considered specifically in this study: the exponential packet

$$A(X) = e^{-|X|}, \qquad \hat{A}(K) = \frac{1}{\pi(1+K^2)} \tag{5}$$

and the Gaussian packet

$$A(X) = e^{-X^2}, \qquad \hat{A}(K) = \frac{e^{-K^2/4}}{2\sqrt{\pi}} \tag{6}$$

The total acoustic power output emitted by the wave packet into the computational box can be expressed as

$$P(l) = \int_{-l/2}^{l/2} \overline{Re(pe^{-it}) \cdot Re(ve^{-it})}|_{y=0}\,\mathrm{d}x \tag{7}$$

where v is the complex velocity in the y direction, normalized in the same way as p. The overbar denotes time averaging, and l is the computational box length in the x direction, which in this case is infinite. Then, $P(l \to \infty)$ can be written by using Eqs. (3) and (4) as

$$P(l \to \infty) = \frac{\pi}{\rho c_0 M_c \varepsilon^2}\int_{-M_c}^{M_c} \hat{A}^2\left(\frac{k-1}{\varepsilon}\right)\sqrt{M_c^2 - k^2}\,\mathrm{d}k \tag{8}$$

Two specific situations are considered; low subsonic and supersonic. In a low-subsonic flow, the main contribution to the sound comes from the wave-number range $k \sim 0$ [see Eq. (4)]; thus, by Eq. (5) or (6), $\hat{A}^2$ of Eq. (8) can be taken as the slow-varying function and the square root of Eq. (8) can be taken as the fast-varying function around $k = 0$. Therefore, by taking $\hat{A}^2$ as a constant with the value of $\hat{A}^2(-1/\varepsilon)$, one gets the asymptotic approximation

$$P(l \to \infty) \sim \frac{\pi^2 M_c}{2\rho c_0 \varepsilon^2}\hat{A}^2(-\varepsilon^{-1}) \tag{9}$$

The condition for Eq. (9) to be valid is

$$\hat{A}\frac{[(\pm M_c - 1)/\varepsilon]}{\hat{A}(-1/\varepsilon)} = \mathcal{O}(1) \tag{10}$$

by the previous argument. For the exponential packet, this yields the condition

$$M_c < \mathcal{O}(1) \tag{11}$$

and for the Gaussian wave packet, the condition

$$M_c/\varepsilon^2 < \mathcal{O}(1) \tag{12}$$

Crighton and Huerre[4] showed that the scales 1 and ε^2 are the integral length scales of the exponential source and the Gaussian source, respectively, where the integral length scale Δ is the smallest scale still fulfilling

$$\int_{-\Delta}^{\Delta} A(\varepsilon x)e^{ix}\,\mathrm{d}x \sim \int_{-\infty}^{\infty} A(\varepsilon x)e^{ix}\,\mathrm{d}x \tag{13}$$

M_c^{-1} is in the order of the sound wavelength in the normalized coordinates that are used here. Thus Eqs. (11) and (12) are the conditions for the sound wavelength to be bigger than the acoustic source integral length scale, meaning the source has to be compact.

For a supersonic flow, the main contribution for the sound comes from the wave-number range $k \sim 1$ because of the form of $A(\varepsilon x)$ [see Eqs. (5) and (6)]. Thus, the square root in the integrand of Eq. (8) is the slow-varying function this time and $\hat{A}^2$ is the fast-varying function. This yields the asymptotic approximation

$$P(l \to \infty) \sim \frac{B_0\sqrt{M_c^2 - 1}}{2\rho c_0 M_c \varepsilon} \tag{14}$$

where B_0 is 1 for the exponential source and $\sqrt{(\pi/2)}$ for the Gaussian source. Similar arguments as in the low subsonic case lead to the condition $M_c > \mathcal{O}(1)$ for Eq. (14) to hold, which yields

$$M_c^{-1}/\varepsilon^{-1} < \mathcal{O}(1) \tag{15}$$

Expression (15) means that the source has to be noncompact for Eq. (14) to hold, because ε^{-1} is in the order of the plain source length scale Θ, defined as the largest length scale still fulfilling

$$A(\varepsilon\Theta) = \mathcal{O}(1) \tag{16}$$

Note the difference between the plain source length scale defined in Eq. (16) and the integral one defined in Eq. (13). It is shown that these two scales also have a significant role in determining the required computational box length.

Large-Scale Model, Finite Box

The assumption that no distortion is created because of the boundary condition leads to the conclusion that the flowfield inside the finite computational box is as if the box were infinite. Thus, by using Eqs. (3) and (7), one can show

$$P(l) = \frac{1}{\rho c_0 M_c \varepsilon^2} \int_{-M_c}^{M_c} \sqrt{M_c^2 - k^2}\, \hat{A}\left(\frac{k-1}{\varepsilon}\right) I \, \mathrm{d}k \qquad (17)$$

$$I \equiv \int_{-\infty}^{\infty} \frac{1}{s-k} \hat{A}\left(\frac{s-1}{\varepsilon}\right) \sin\left(\frac{s-k}{2} l\right) \mathrm{d}s \qquad (18)$$

For $l \to \infty$, I can be shown to be $\pi \hat{A}[(k-1)/\varepsilon]$ and Eq. (17) becomes identical to Eq. (8). Thus, the rate of convergence of Eq. (17) to Eq. (8) is determined by the effect of l on I. If $\hat{A}[(s-1)/\varepsilon]$ varies slowly enough about $s = k$, then I will have the asymptotic value as the analytical value when $l \to \infty$. For a low-subsonic flow, it was shown that most of the sound comes from $k \sim 0$ and $\hat{A}$ changes on a scale relative to the integral length scale. Therefore, l should be bigger than the integral length scale for Eq. (17) to converge to Eq. (8), which yields

$$l > \mathcal{O}(1), \qquad M_c < \mathcal{O}(1) \qquad (19)$$

for the exponential source and

$$\varepsilon^2 l > \mathcal{O}(1), \qquad M_c/\varepsilon^2 < \mathcal{O}(1) \qquad (20)$$

for the Gaussian source, which agrees with Crighton's[5] estimate for a low-subsonic Gaussian source.

For a supersonic flow, it was shown that most of the sound comes from $k \sim 1$ and $\hat{A}$ changes on a scale relative to the plain source length scale. Thus, l should be bigger than the plain source length scale, which yields

$$\varepsilon l > \mathcal{O}(1) \qquad (21)$$

which agrees with Mitchell et al.'s[6] estimate for their particular case.

Results

The integral (17) was evaluated according to the method of Blakemore et al.[7] $P(l)$ is compared to $P(l \to \infty)$ using Eqs. (17) and (8) for the exponential source and the Gaussian source in Figs. 2a and 2b, respectively. The value for $\varepsilon = 0.2$ was chosen as typical from Laufer and Yen's[2] experiment. It is seen that if the computational box is too short, the acoustic source may appear as an acoustic sink, as in the low-subsonic case. It is also clear that $P(l)$ converges faster to $P(l \to \infty)$ as M_c increases from low subsonic to supersonic, whereas $M_c > 1$ the convergence rate is quite independent of M_c. That is because the sound for subsonic flow is created only by the amplitude variation of the packet. Therefore, the computational box has to be long enough to contain enough information on that variation. For a supersonic flow, the sound appears mainly as a Mach wave created by the fluctuations inside the wave packet; thus the box has to contain just enough cycles of these fluctuations. The last requirement is expressed in Eq. (21), which seems to be sufficient by Figs. 2a and 2b. However, for the low-subsonic flow, the requirement that l should be bigger than the integral length scale as in Eqs. (19) and (20) seems to be sufficient only for the Gaussian source and not for the exponential source. Because for the exponential source the low-subsonic requirement (19) is less restrictive than the supersonic requirement (20). Actually, I of Eq. (17) can be evaluated exactly for the exponential source by Cauchy's residue theorem, and it can be shown that, for low-subsonic flow, one has to require

$$\varepsilon l|_{\min} = -2 \ln(\varepsilon E_r) \qquad (22)$$

instead of Eq. (19) for the exponential source, where E_r is the expected relative error in the power output. For $\varepsilon = 0.2$ and $E_r = 5\%$, one gets $\varepsilon l|_{\min} = 9.21$, which agrees with the result of Fig. 2a.

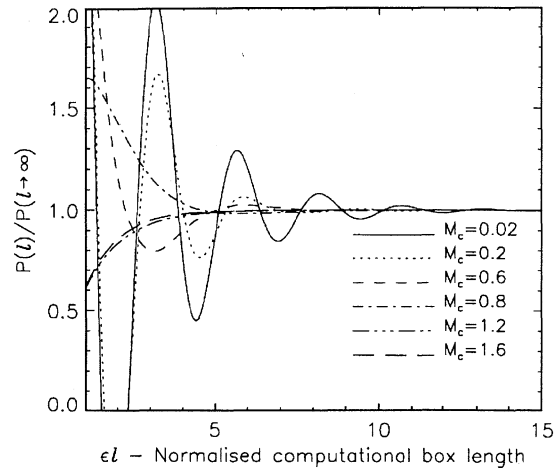

a) Exponential wave packet

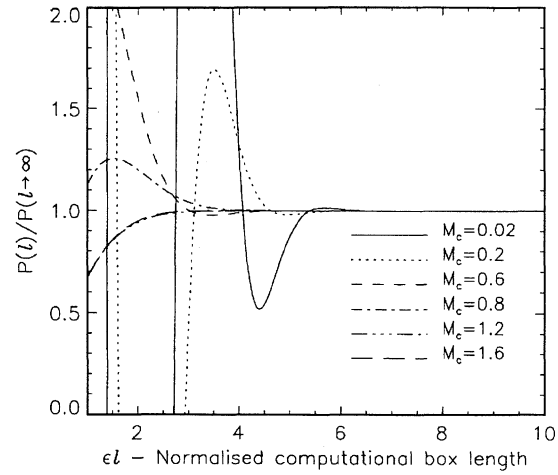

b) Gaussian wave packet

Fig. 2 Variation of the normalized acoustic power output with the normalized computational box length $\varepsilon = 0.2$.

Concluding Remarks

This study presented an estimate for the computational box length scale needed for an accurate estimate of the total acoustic power output emitted by a large-scale structure in the form of a wave packet. The model shows that two different scales dominate the sound production: the source integral length scale for the low-subsonic case and the plain source length scale for the supersonic case. Thus, the computational box length must be bigger than each length scale in its dominant region. However, it was found that for the low-subsonic case this is only a necessary condition but not necessarily a sufficient one. The work showed that the low-subsonic case is expected to be the most problematic, in terms of the sound level [see Eqs. (9) and (14)] and in terms of the required computational box length. Given that classic acoustics has the distance from the acoustic source to the start of the far field being greater than the sound-wave length scale M_c^{-1}, it is increasingly difficult at low M_c to compute the sound directly. Use of an indirect method based on an acoustic analogy will be presented by the authors in the near future.

Acknowledgment

This study was supported by British Aerospace (operations) Limited, Sowerby Research Centre.

References

[1]Kibens, V., "Discrete Noise Spectrum Generated by an Acoustically Excited Jet," *AIAA Journal*, Vol. 18, No. 4, 1980, pp. 434–441.

[2]Laufer, J., and Yen, T. C., "Noise Generation by a Low Mach Number Jet," *Journal of Fluid Mechanics*, Vol. 134, Sept. 1983, pp. 1–31.

[3]Ffowcs Williams, J. E., and Kempton, A. J., "The Noise from the Large Scale Structure of a Jet," *Journal of Fluid Mechanics*, Vol. 84, No. 4, 1978, pp. 673–694.

[4]Crighton, D. G., and Huerre, P., "Shear Layer Pressure Fluctuations and Superdirective Acoustic Sources," *Journal of Fluid Mechanics*, Vol. 220, Nov. 1990, pp. 355–368.

[5]Crighton, D. G., "Computational Aeroacoustics for Low Mach Number Flows," *Computational Aeroacoustics*, Springer–Verlag, New York, 1993, pp. 50–68.

[6]Mitchell, B. E., Lele, S. K., and Moin, P., "The Direct Computation of Mach Wave Radiation in an Axisymmetric Supersonic Jet," AIAA Paper 96-1729, May 1996.

[7]Blakemore, M., Evans, G. A., and Hyslop, J., "Comparison of Some Methods for Evaluating Infinite Range Oscillatory Integrals," *Journal of Computational Physics*, Vol. 22, No. 3, 1976, pp. 352–396.

S. Glegg
Associate Editor

Crossflow Vortices of a Jet Injected into a Supersonic Crossflow

Juan Gabriel Santiago* and J. Craig Dutton†
University of Illinois at Urbana–Champaign, Urbana, Illinois 61801

Introduction

NUMEROUS investigations of the fluid mechanics of the transverse jet injected into a supersonic flow (TJISF) flowfield have been motivated by the study of supersonic combustor fuel injection, thrust vector control of rocket nozzles, and jet reaction force prediction. Early studies presented detailed qualitative discussions of the structure of the TJISF flowfield.[1,2] A few studies have provided either quantitative or semiquantitative measurements of the velocity fields of underexpanded jets injected into a supersonic flow.[3–5] Despite these investigations, there is a dearth of nonintrusive, quantitative mean velocity and turbulence measurements in the TJISF flowfield. This Note uses laser Doppler velocimetry (LDV) measurements of the mean velocity fields to study development of the crossflow vortices of a sonic, underexpanded transverse jet injected into a Mach 1.6 crossflow. These measurements add to the current understanding of this flowfield and aid in modeling efforts. This investigation is part of a larger experimental study of the mean and turbulent velocity field of a TJISF.[5]

A typical underexpanded TJISF flowfield is shown schematically in Fig. 1. The figure depicts the supersonic freestream flow with the jet injected through the bottom wall. The obstruction caused by the jet generates a bow shock in the freestream (not shown). After leaving the orifice, the jet expands through a Prandtl–Meyer fan and then compresses through a barrel shock and Mach disk. Downstream of the Mach disk, the jet plume is quickly turned downstream. Furthermore, the TJISF flowfield contains a counter-rotating crossflow vortex pair in the jet plume. This vortex action is the primary source of jet entrainment and dominates the jet's downstream velocity field.[2] Other vortical structures present in the TJISF flowfield include the horseshoe vortex that wraps around the windward side of the jet and trails downstream, shear layer vortices that form around the circumference of the jet (not shown in Fig. 1), and wake vortices periodically shed near the base of the inner jet core.

Received Aug. 9, 1996; revision received Dec. 17, 1997; accepted for publication Jan. 25, 1997.

*Graduate Research Assistant, Department of Mechanical and Industrial Engineering; currently Senior Member, Technical Staff, Spacecraft Thermal Department, The Aerospace Corporation, El Segundo, CA 90245. Member AIAA.

†Professor, Department of Mechanical and Industrial Engineering. Associate Fellow AIAA.

Experimental Facility and Diagnostics

The experiments described here used the transverse jet facility of the Gas Dynamics Laboratory at the University of Illinois at Urbana–Champaign. During the experiments, the facility's wind tunnel was run at the Mach 1.6 design condition with a stagnation pressure of 241 kPa and a stagnation temperature of 295 K (resulting in a unit $Re = 58.8 \times 10^6$ m^{-1}). A sonic, underexpanded jet with a 4-mm exit diameter (d) was injected into the test section through a window in the bottom wall of the wind tunnel. The jet stagnation pressure, stagnation temperature, jet-to-crossflow momentum flux ratio, and Reynolds number based on jet diameter for the current study are as follows: $P_{oj} = 476$ kPa, $T_{oj} = 300$ K, $J = 1.7$, and $Re_d = 1.1 \times 10^5$.

A frequency preshifted two-component LDV system was used to measure three mean velocity components, U, V, and W, as well as five of the six kinematic Reynolds stresses, $\langle u'^2\rangle$, $\langle v'^2\rangle$, $\langle w'^2\rangle$, $\langle u'v'\rangle$, and $\langle u'w'\rangle$, throughout the x–y midline plane and two y–z planes (i.e., crossflow planes; see Fig. 1). Velocity measurements were obtained at more than 4000 spatial locations with four optical setups. Also, 4000 instantaneous velocity realizations were obtained at each location to minimize statistical uncertainty. An analysis of the error associated with the LDV measurements was presented previously.[5] The crossflow plane mean V–W measurements presented here are accurate to within ±1% of the upstream crossflow velocity, $U_c = 446$ m/s, at the 95% confidence level and were located within $\pm 0.0125d$ (i.e., ±50 μm) in a measurement grid spaced a distance of $0.125d$ (0.5 mm) in both the spanwise and transverse directions.

Results and Discussion

Figure 2 shows the V–W velocity vectors of half of the crossflow planes at $x/d = 3$ and 5 superimposed on contours of the dimensionless mean streamwise vorticity field $\zeta_x d/U_c$, where

$$\frac{\zeta_x}{U_c/d} = \frac{d}{U_c}\left[\frac{\partial W}{\partial y} - \frac{\partial V}{\partial z}\right] \tag{1}$$

At these x locations, the center-of-rotation velocities are within 2 deg of the streamwise direction. The vorticity fields are dominated by one of the pair of counter-rotating crossflow vortices of the jet plume. At $x/d = 3$, the vorticity contours are roughly kidney shaped, with large gradients near the bottom left and top right of the vortex cross section. These kidney shapes are longest along a line approximately 27 deg from the z axis. At $x/d = 5$, where the vortices have risen away from the wall and moved apart, the vorticity contours have approximately equal radial gradients around their periphery and are roughly elliptical with the major axis aligned with the y direction. This change in the shape of the mean vorticity contours strongly suggests that the motion of each crossflow vortex is, at first, constrained by the other vortex and by the wall and then behaves more as free vortex as it lifts away from the wall. Also, note that for both $x/d = 3$ and 5, the centers of rotation of the in-plane vectors correspond only roughly to the location of maximum $\zeta_x d/U_c$.

The in-plane velocity vectors also show this constraint of the motion of the crossflow vortices. First, in both crossflow planes, the largest measured V–W velocities and in-plane velocity gradients occur in the constrained regions below the vortex center and between the vortex center and the symmetry plane. The unconstrained regions of the vortex (above and outside the vortex center) are much larger and have smaller velocity magnitudes and smaller velocity gradients. As the plume develops from $x/d = 3$ to 5, its cross-sectional area increases mostly in the transverse direction, and the magnitudes and gradients of the in-plane velocities in the constrained regions are significantly reduced. For example, at $x/d = 3$, the largest measured spanwise velocity in the constrained region below the vortex center is $W = -239$ m/s. At $x/d = 5$, the largest measured spanwise velocity in this region is $W = -119$ m/s. Also, note the difference in the spanwise extent of regions of $\zeta_x d/U_c > 0.1$ for the two crossflow planes. The integrated strengths of the crossflow plane vortices at $x/d = 3$ and 5 are 1.11 and 1.00 m^2/s, respectively.[5]

A significant difference between the vortices of this highly three-dimensional and compressible TJISF flowfield and that of a simple, plane, incompressible, two-vortex flowfield is the nature of the